Volume 17, Number 4, 2024. pp. 453-459

Jordan Journal of Physics

ARTICLE

Structural, Optical, and Electrical Properties of Undoped and Zn-Doped $CaSnO_3$ Nanoparticles Synthesized by the Co-Precipitation Method

V. Balasundaram[a], **V. Balasubramanian**[b], **J. Henry**[c], **T. Daniel**[d], **K. Mohanraj**[e,f] and **G. Sivakumar** [a]

[a]*CISL, Department of Physics, Annamalai University, Chidambaram, Tamil Nadu, India.*
[b]*Department of Science & Humanities, P.S.N. College of Engineering and Technology, Tirunelveli-627152, India.*
[c]*Department of Physics, School of Engineering & Technology, Dhanalakshmi Srinivasan University, Trichy – 621 112, India.*
[d]*Department of Physics, MVJ College of Engineering, Bengaluru, Karnataka-560067, India.*
[e]*Department of Physics, Manonmaniam Sundaranar University, Tirunelveli, Tamil Nadu, India.*
[f]*Department of Physics, School of Basic and Applied Sciences, Central University of Tamil Nadu Thiruvarur, Tami l Nadu 61 0 005, India.*

***Doi:*https://doi.org/10.47011/17.4.8**

Received on: 17/02/2023; *Accepted on: 18/06/2023*

Abstract: In this work, we studied the optical properties of undoped and Zn-doped $CaSnO_3$ nanoparticles. XRD patterns revealed the formation of the orthorhombic $CaSnO_3$ structure, with a pronounced shift for doped samples. Fourier-transform infrared spectroscopy identified the presence of Ca-O and Sn-O vibrations. The bandgap of CaSnO3 was found to be 4.5 eV, with variations observed upon doping. Scanning electron microscopy images showed a polygonal morphology with size variations. In Zn doped Zn-doped $CaSnO_3$, PL spectra showed a peak shift towards the visible region compared to the undoped sample. Among the Zn concentrations, 0.02M Zn-doped $CaSnO_3$ exhibited specific capacitance of 2880 F/g, as measured from the CV curve.

Keywords: Zn doped $CaSnO_3$, Co-precipitation, Structural properties, Optical properties, Electrical properties.

Introduction

Luminescent materials have attracted significant attention because of their potential applications in various fields, including photocatalysis, solar cells, and biomedicine. $CaSnO_3$ is a promising luminescent material due to its chemical stability, low cost, and non-toxicity. Luminescent properties of $CaSnO_3$have been enhanced by doping with several rare earth elements (e.g.Sm, Nd, Er, Eu, Tm, Yb, Pr, and Tb) [1-7]. In recent years, researchers have focused on $CaSnO_3$ particles doped with transition metals for applications such as batteries [8], efficient photocatalysts for the degradation of organic dye [9], piezoelectric properties for high-temperature applications [10], magnetic and electrochemical applications [11], photocatalytic activity [12], and memory devices [13]. Manoharan *et. al.,* recently reported that hafnium (Hf^{4+})-doped $CaSnO_3$ perovskites exhibit a co-existence of

Corresponding Author: G. Sivakumar **Email**: gskdopcisl@gmail.com

ferromagnetic and diamagnetic nature [14]. To the best of our knowledge, there are few studies available on supercapacitor applications of $CaSnO_3$ nanoparticles [15,16]. Hence, in the present work, we study the effect of doping by Zn on the structural, optical, morphological, and electrochemical properties of $CaSnO_3$ particles.

Experimental Methods

Undoped and Zn-doped $CaSnO_3$ nanoparticles (with various Zn concentrations of 0.01, 0.02, and 0.03 M) were prepared by the co-precipitation method using $CaCl_2$, $SnCl_2.2H_2O$, NaOH, and $ZnCl_2$ precursors. First, 0.4M $SnCl_2.2H_2O$ and 0.8M $CaCl_2$ were mixed well with the assistance of a magnetic stirrer. Next, a 4M NaOH solution was added dropwise to the former solution (pH 12). The whole solution was stirred at 65˚C for 45 min and then filtered, washed, and dried for 24 hours. The resulting product was at 900˚C for 6 hours. For Zn-doped $CaSnO_3$ appropriate amount of $ZnCl_2$ was added into the precursor solution.

The structural, molecular vibrational, surface, optical, and electrical properties of undoped and Zn doped $CaSnO_3$ nanoparticles were examined by PANalytical XPERT-PRO diffractometer (λ=1.5406 Å; 10˚-80˚) patterns, PerkinElmer FTIR spectrometer (Spectrum Two, Model C92107, resolution 4cm^{-1}) spectra, CARL ZEISS (EVO 18) scanning electron microscopy, Shimadzu (UV-2700) UV-visible spectroscopy (200-800 nm), and electrochemical workstation (CH 1604E; three-electrode system) CV, respectively.

Results and Discussion

The XRD pattern of Undoped $CaSnO_3$ nanoparticles, calcined at 900 ºC, is given in Fig. 1(a). The XRD pattern exhibits a prominent peak at 2θ=32.08°, corresponding to the (*112*) plane of the polycrystalline orthorhombic $CaSnO_3$, consistent with the JCPDS card No.77-1797. Some sharp peaks are detected at 2θ 46.04°(*004*), 22.57°(*002*), 56.60°(*132*), and 57.55°(*312*), which also match theJCPDS card No.77-1797. For Zn-doped samples, the major crystalline peak is shifted to a lower 2θ, indicating the incorporation of Zn into the $CaSnO_3$ lattice.

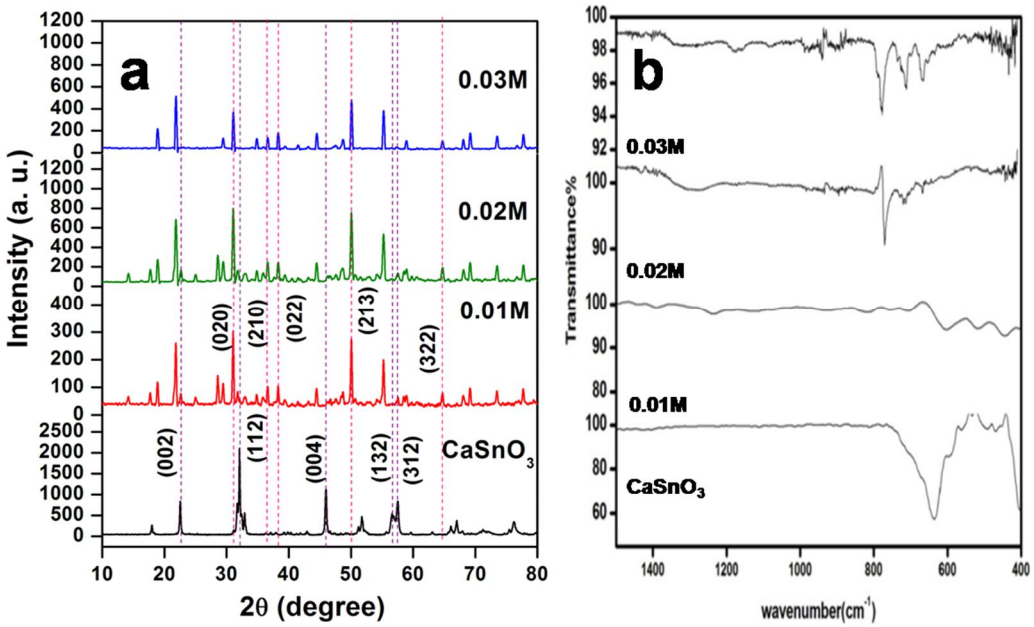

FIG.1. Zn-doped $CaSnO_3$ nanoparticles (a) XRD patterns and (b) FTIR spectra.

The average crystallite size (D) was calculated using the Scherrer formula [17]:

$$D = \frac{k\lambda}{\beta \cos\theta} \quad (1)$$

where k =0.9, λ =1.5406Å, β is the FWHM, and θ the diffraction angle.

Dislocations are imperfections in a crystal, associated with the misregistry of the lattice in one part of the crystal with respect to another part. Unlike vacancies and interstitial atoms, dislocations are not equilibrium imperfections [17]. In fact, the growth mechanism involving dislocations is a matter of importance. The

dislocation density (δ) was calculated by using the formula:

$$\delta = \frac{1}{D^2} \quad (2)$$

Stresses in the film are one of the most important unfavorable factors affecting the structural properties and can result from a geometric mismatch at boundaries between the crystalline lattices of the films and the substrate [18]. These stresses can cause microstrain (ε) in the films, calculated using the formula

$$\varepsilon = \frac{\beta cos\theta}{4} \quad (3)$$

The crystallite size was found to be 50 nm for undoped $CaSnO_3$, 0.01 M, and 0.02 M Zn-doped $CaSnO_3$ nanoparticles. For 0.03M Zn-doped $CaSnO_3$, however, it approximately doubled to 98 nm. The higher crystallite size is useful for photovoltaic applications. A similar trend is reflected in the dislocation density and microstrain values, as shown in Table 1. The dislocation density and microstrain increased with an increase in doping upto 0.02 M and then decreased for 0.03 M Zn-doping. This indicates improvement in the crystalline nature of the nanoparticles.

TABLE 1. Crystalline size, dislocation density, and microstrain in the undoped and Zn-doped $CaSnO_3$nanoparticles.

Sample	Concentration	Crystallite size (nm)	Dislocation density (10^{15})	Microstrain (10^{-3})
Undoped CaSnO3	-	50	0.39	0.68
Zn-doped CaSnO3	0.01M	50	0.40	0.68
	0.02M	49	0.41	0.69
	0.03M	98	0.10	0.34

The vibrational characteristics of the undoped and Zn-doped $CaSnO_3$ nanoparticles are shown in Fig. 1(b). Some weak bands appear around 400-670 cm^{-1} and a strong band is observed at 635 cm^{-1}, attributed to the presence of Sn-O stretching vibrations [19, 20]. The peak appearing at 564 $cm^{-1}$is due to Ca-O vibrations. FTIR analysis confirms the presence of metal oxide vibrations, consistent with findings in the literature. For 0.01 M Zn $CaSnO_3$ nanoparticles, FTIR peaks reappear around 630 cm^{-1}, 485 cm^{-1}, 1619 cm^{-1}, and 1286 cm^{-1},owing to SnO_6 vibrations, Zn-O stretching, C–H stretching vibration, and carbonate vibrations, respectively [20-22]. Similarly, 0.02 M and 0.03M Zn-doped $CaSnO_3$ nanoparticles show peaks around 485 and 670 cm^{-1}, due to the Zn-O vibrations, further confirming the incorporation of Zn into CaSnO3 lattice, as shown in the XRD patterns.

The optical characteristics of undoped and Zn-doped $CaSnO_3$ nanoparticles are shown in Fig. 2. It is observed that $CaSnO_3$ nanoparticles reach maximum absorbance at 245 nm. This result is in agreement with the report on $CaSnO_3$ nanoparticles [19]. Upon Zn doping, the absorption shifts toward shorter wavelengths, indicating a blue shift for all Zn concentrations compared to $CaSnO_3$. Additionally, the absorbance slightly decreases in the visible region.

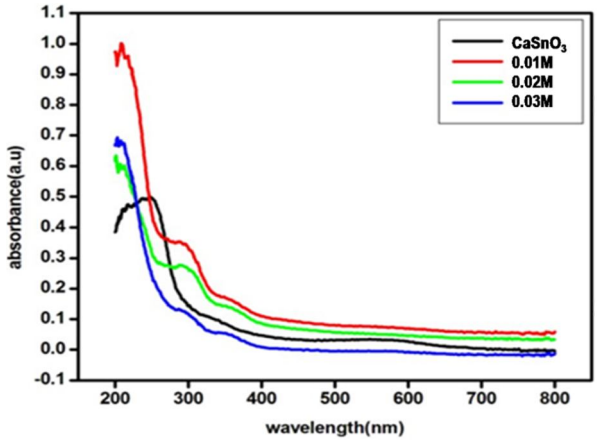

FIG.2. UV absorption spectrum for the undoped and Zn-doped $CaSnO_3$ nanoparticles.

The bandgap energy was calculated by the following equation:

$$(\alpha h\upsilon) = A\left(h\upsilon - E_g\right)^n \quad (4)$$

where 'a' is the absorption coefficient, 'hυ' is photon energy, 'A' is a parameter that depends on the transition probability, 'h' is Planck's constant, and the exponent 'n' depends on the nature of the transition during the absorption process. The value of n is 1/2, 3/2, 2, and 3 for direct allowed, direct forbidden, indirect allowed, and indirect forbidden transitions, respectively [23].

Previous experimental and theoretical studies indicated that $CaSnO_3$ is a direct bandgap semiconductor [24, 25]. Hence, in this work, we use n = ½, consistent with $CaSnO_3$ direct bandgap semiconductor nature. The bandgap of the $CaSnO_3$ sample was found to be 4.5 eV, aligning closely with the 4.2eV value reported by Mizoguchi *et al.* [26] and Sumithra *et al.* [27,]. For Zn-doped $CaSnO_3$ concentrations 0.01, 0.02, and 0.03 M, the bandgaps are approximately 4.9 , 3.7, and 5.0 eV, respectively. The spectra show a blue shift for all concentrations compared to undoped $CaSnO_3$ nanoparticles due to increased crystallite size. The blue shift is attributed to the Burnstein–Moss effect [28]. The donor Zn atoms provide additional carriers that shift the Fermi level into the conduction band so that the energy gap becomes larger. The optical absorption is slightly changed by increasing the Zn concentration as reflected in bandgap energy.

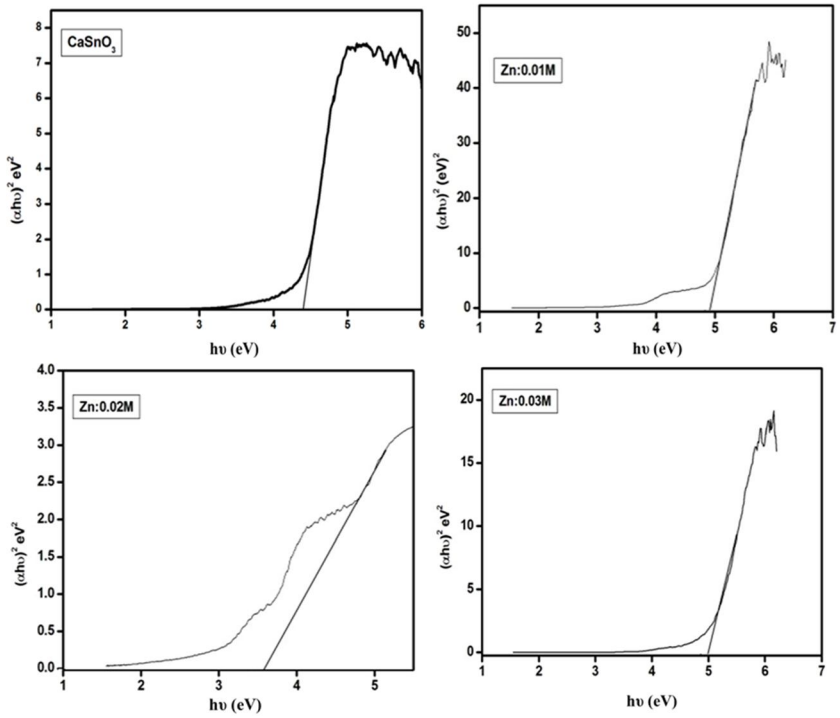

FIG. 3. Tauc plots for the undoped and Zn-doped $CaSnO_3$ nanoparticles.

SEM images of Zn-doped $CaSnO_3$ particles are shown in Fig. 4. All samples show a flower-flake-like morphology attached to each other. The average size is approximately 1.6 μm.

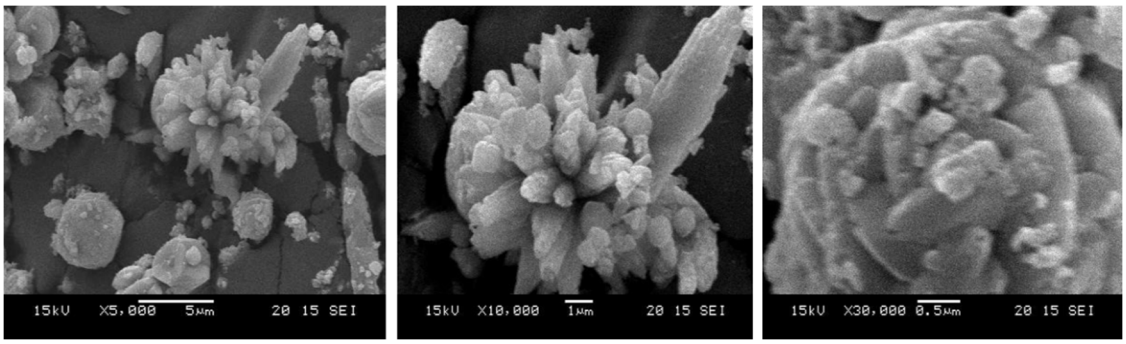

FIG. 4. SEM images of Zn-doped $CaSnO_3$ nanoparticles.

The photoluminescence (PL) properties, recorded with the excitation λ = 245nm, are shown in Fig. 5. An emission peak appears at 305 nm for the undoped $CaSnO_3$ nanoparticles. The possible defects that contribute to PL characteristics are oxygen vacancies. Secondary emission peaks at 408 and 431 nm, attributed to oxygen defects, exhibit blue emission properties [27]. For the Zn-doped samples, the emission peak is observed at 310 nm, showing a red shift compared to undoped $CaSnO_3$.

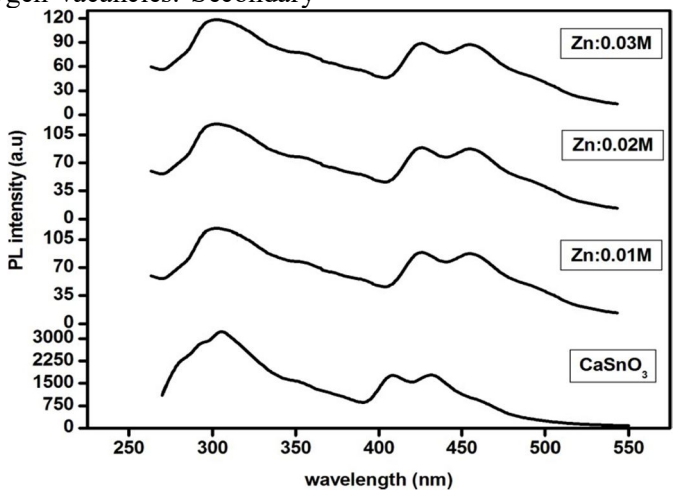

FIG.5. PL emission spectra of $CaSnO_3$ and Zn(0.01, 0.02, and 0.03M) doped CaSnO3 nanoparticles.

The CV measurements for Zn-doped $CaSnO_3$ nanoparticles (scan rates: 10, 50, 100,and 200 mV/s in 0.5M Na_2SO_4 solution; potential range: -1.6 to +1.6V vs Ag/AgCl electrode) are shown in Fig. 6. For the undoped sample (scan rate of 10 mVs^{-1}) an oxidation peak is observed at 0.92 V, and a redox peak is seen at -0.61 V. Anodic and cathodic peaks appear at -0.29 V and -0.63 V, respectively. It is noticed that the peak shifted towards a high potential with respect to scan rate. From the measurements, the specific capacitance was calculated according to the early report [29].

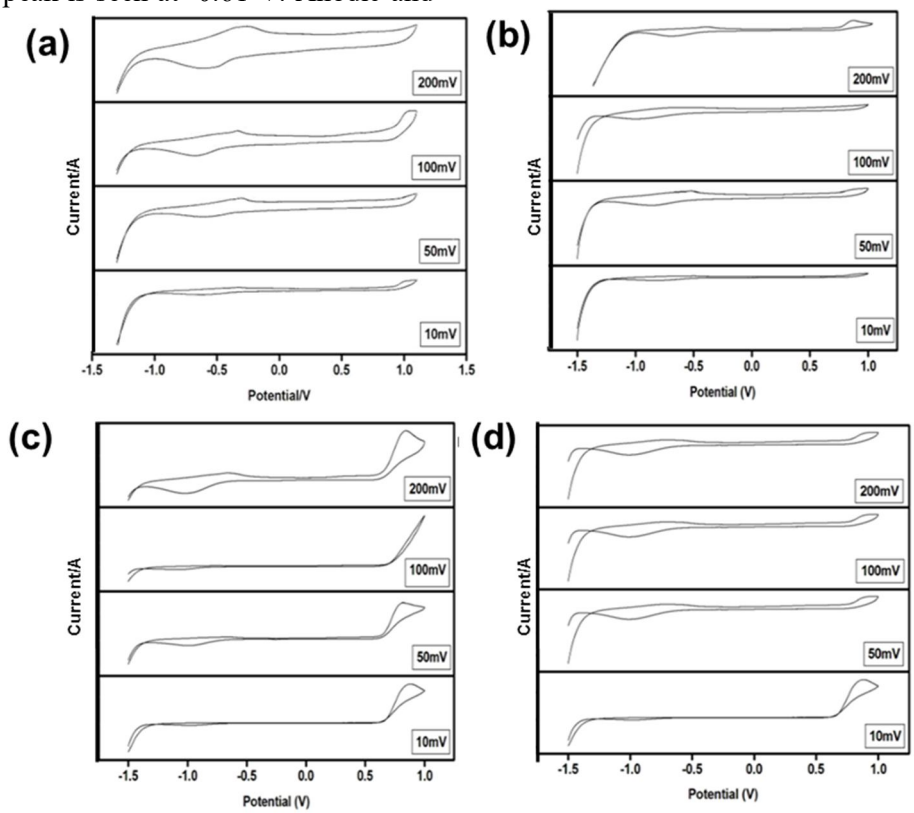

FIG.6. CV data of (a) $CaSnO_3$, (b) 0.01M, (c) 0.02M, and (d) 0.03M Zn-doped CaSnO3 nanoparticles.

At a scan rate of 10 mV s^{-1}, the $CaSnO_3$ nanoparticles have a specific capacitance of about 572 F/g, decreasing with increasing scan rates (167.2 F/g at 50mV/s, 94.6 F/g at100mV/s, and 71.1 F/g at 200mV/s). For Zn-doped $CaSnO_3$ (0.01, 0.02, and 0.03 M), the CV curves display varying loop shapes with changing Zn concentrations.The specific capacitances at 10 mV/s are 634 F/g, 2860 F/g, and 2880 F/g, respectively, decreasing similarly with higher scan rates. Among the samples, the 0.02 M and 0.03 M Zn-doped samples exhibit the highest capacitance values, suggesting that Zn-doped $CaSnO_3$ is an effective supercapacitor electrode material.

Conclusion

This paper reports on the structural, molecular vibrational, surface, optical, and electrical properties of Zn-doped $CaSnO_3$ nanoparticles synthesized via the co-precipitation method. XRD analysis confirms the formation of an orthorhombic $CaSnO_3$. The polycrystalline peak shift indicates the incorporation of Zn in the $CaSnO_3$ lattice. Fourier transform infrared spectroscopy identified the presence of Ca-O, Sn-O, and Zn-O vibrations at 564, 635, and 485 cm^{-1}, respectively. Optical absorption spectra show a blue shift across all Zn doped concentrations compared to the undoped sample, with absorption in the visible region decreasing as Zn concentration increases. The bandgap of for the $CaSnO_3$ is 4.5 eV, , while Zn doping yields bandgaps of 4.9, 3.7,and 5.0 eV for Zn concentrations of 0.01, 0.02, and 0.03 M, respectively. SEM images depict Zn-doped particles as flower-flake-like structures with an average size of 1.6µm. In Zn-doped $CaSnO_3$, PL spectra show a peak shift towards the visible region compared to the undoped $CaSnO_3$.CV analysis identifies Zn-doped $CaSnO_3$ with 0.02 M and 0.03 M Zn as optimal for use as supercapacitor electrodes.

References

[1] Gordo, V.O., Arslanli, Y.T., Canimoglu, A., Ayvacikli, M., Gobato, Y.G., Henini, M., and Can, N., Appl. Radiat. Isot., 99 (2015) 69.

[2] Saha, S., Das, S., Ghorai, U.K., Mazumder, N., Ganguly, D., and Chattopadhyay, K.K., J. Phys. Chem. C., 119 (2015) 16824.

[3] Pang, X.L., Jia, C.H., Li, G.Q., and Zhang, W.F., Opt. Mater., 34 (2011) 234.

[4] Stanulis, A., Katelnikovas, A., Bael, V.M., Hardy, A., Kareiva, A., and Justel, T., J. Lumin., 172 (2016) 323.

[5] Hu, Y., Zhou, F., Tian, X., Ji, C., Huang, Z., Wen, J., Luo, F., Chen, Z., Liu, X., and Peng, Y., Spectrochim. Acta A Mol. Biomol. Spectrosc., 243 (2020) 118799.

[6] Jin, Y., Hu, Y., Chen, L., Wang, X., Ju, G., and Mu, Z., J. Lumin., 138 (2013) 83.

[7] Stanulis, A., Katelnikovas, A., Enseling, D., Dutczak, D., Sakirzanovas, S., Bael, M.V., Hardy, A., Kareiva, A., and Justel, T., Opt. Mater., 36 (2014) 1146.

[8] Antonio, J.E., Rosas-Huerta, J.L., Cervantes, J.M., Flores, J.L., Romero, M., Carvajal, E., and Escamilla, R., Comput. Mater. Sci., 219 (2023) 112006.

[9] Venkatesh, G., Prabhu, S., Geerthana, M., Baskaran, P., Ramesh, R., and Prabhu, K.M., Optik, 212 (2020) 164716.

[10] Chen, X., Gao, P., Liu, C., Zhang, K., Huang, X., Zhang, H., Zhang, F., and Pu, Y., Céram. Int., 49 (2022) 1436.

[11] Bhat,A.A. and Tomar, R., J. Alloys Compd., 876 (2021) 160043.

[12] Wang, J., Asakura, Y., Hasegawa, T., and Yin, S., J. Environ. Chem. Eng., 10 (2022) 108169.

[13] Kumar,A., Khan,B., Singh,G., Dixit,A., Upendra Kumar, U., and Singh, M.K.,Phys. Scr., 95 (2020) 105807.

[14] Manoharan, A., Suresh, B., Kumari, A., Munisamy, M., and Krishnan, S., Solid State Commun., 360 (2023) 115033.

[15] Sharma, N., Shaju, K.M., Rao, G.S., and Chowdari,B.V.R., Electrochem. Commun.,12 (2002) 947.

[16] Sharma, Y., Sharma, N., Subba Rao, G.V., and Chowdari, B.V.R., Chem. Mater., 21 (2008), 6829.

[17] Turgut, G., Keskenler, E.F., Ayd, S., Dogan, S., Duman, S., Özçelik, S., Gürbulak, B., and Esen, B., Phys. Status Solidi A, 211 (2014) 580.

[18] Pradip, K.K., Sarma, B.K. and Das, H.L., Bull. Mater. Sci., 23 (2000) 313.

[19] Moshtaghi, S., Salavati-Niasari, M., and Ghanbari, D.,J. Nanostruct.,5 (2015) 169.

[20] Lucena, G.L., de Lima, L.C., Honório, L.M.C., de Oliveira, A.L.M., Tranquilim, R.L., Longo, E., and dos Santos, I.M.G., Cerâmica, 63(2017) 536.

[21] Parthasarathi, V. and Thilagavathi, G., Int. J. Pharm. Pharm. Sci., 3 (2011) 392.

[22] Kavitha, S., Dhamodaran, M., Prasad, R., and Ganesan, M., Int. Nano Lett., 7 (2017) 141.

[23] Hussein, H.F., Walailak J., Sci.& Tech., 11 (2014) 413.

[24] Shaili, H., Salmani, E., Beraich, M., Zidane, M., Taibi, M., Rouchdi, M., Ez-Zahraouy, H., Hassanain, N., and Mzerd, A., ACS Omega, 6 (2021) 32537.

[25] Tsega, M.and Dejene, F. B., Bull. Mater. Sci., 40(2017) 1347–1354.

[26] Mizoguchi, H., Eng, H.W., and Woodward, P.M., Inorg. Chem, 43 (2004) 1667.

[27] Sumithra, S. and Jaya, N.V., J. Mater. Sci. Mater. Electron., 29 (2018) 4048.

[28] Khan, M.A.M., Kumar, S., Khan, M.N., Ahamed, M. and Dwayyan, A.S.A., J. Lumin., 155 (2014) 275.

[29] Navale, S.T., Mali, V., Pawar, S.A., Mane, R.S., Naushad, M., Stadler, F.J., and Patil, V.B., RSC Adv., 5 (2015) 51961.